RSC Advances

PAPER

View Article Online
View Journal | View Issue

Cite this: *RSC Adv.*, 2021, **11**, 6472

A new pH/NIR responsive theranostic agent for magnetic resonance imaging guided synergistic therapy†

Yechao Du,[a] Daguang Wang,[a] Shuo Wang,[b] Wei Li*[a] and Jian Suo *[a]

Received 10th November 2020
Accepted 26th January 2021

DOI: 10.1039/d0ra09538a

rsc.li/rsc-advances

New nano-reagents with diagnostic imaging and therapeutic functions are very important for precision medicine against cancer. In this work, a new nanotheraontic agent for magnetic resonance imaging (MRI) guided combined photothermal therapy (PTT) and chemotherapy was constructed based on polydopamine (PDA) functionalized copper ferrite nanospheres (PDA@CFNs). The high relaxivity makes it possible for PDA@CFNs to become a promising MRI contrast agent, providing necessary and exhaustive information for tumor diagnosis. In addition, because both CFNs and PDA have strong near-infrared (NIR) absorption, PDA@CFNs exhibit excellent photothermal performance. Highly effective tumor ablation is achieved in a mouse model through PTT and pH/NIR triggered on-demand chemotherapy. These findings reveal that constructing smart pH/NIR responsive multifunctional theranostic agents is a feasible strategy for precision cancer therapy.

Introduction

Cancer is one of the leading causes of death in the world.[1,2] Therefore, exploring anti-cancer treatment methods with a high effectiveness is the focus of current research. Chemotherapy is currently one of the main cancer treatments, but the intrinsic deficiencies of chemical drugs, including poor solubility, fast degradation, and serious side effects to healthy tissues/organs, result in unsatisfactory treatment effect.[3,4] Benefiting from the rapid advances in nanoscience and nanomedicine, stimuli-responsive drug delivery nanosystems have emerged as promising alternatives for on-demand chemotherapy,[5–9] which exert anti-cancer effects through various internal/external stimuli like pH,[10,11] enzymes,[12] redox-responsiveness,[13] temperature, light,[14–16] and magnetic fields. In recent years, many efforts have been devoted to constructing drug delivery nanosystems stimulated by the tumor microenvironment,[17–19] showing high specificity, high therapeutic efficacy, and fewer side effects. In addition, drug delivery nanosystems present some unique features against tumor microenvironments, such as low blood vessel density, hypoxia, weak acidity, redox-responsiveness, and enzyme overexpression. They are extremely important in regulating tumor occurrence, proliferation and metastasis.[20–22] However, with the use of chemotherapy on its own, it is difficult to achieve satisfactory outcomes.

Photothermal therapy (PTT), as a minimally invasive alternative therapy for traditional cancer treatment, has received widespread attention because of its high accuracy and good safety for normal tissues.[23–25] Currently, many nanomaterials with robust absorption of near-infrared (NIR) and high light-to-heat conversion efficiency have been efficaciously used for PTT as photothermal agents, such as colloidal gold nanoparticles, as either gold nanorods, gold nanoshells,[26,27] copper sulfide nanoparticles,[28,29] Mo-based polyoxometalate (POM) nanoparticles,[30] carbon nanotubes[31,32] or palladium nanosheets.[33,34] However, their further clinical applications have been limited owing to the long-term safety. Polydopamine (PDA) has been considered as the next generation of PTT agent due to its good biodegradability, absence of long-term toxicity and high photothermal conversion efficiency (~40%).[35,36] Crucially, the active shell of PDA serves as a good carrier for chemotherapy drugs[37,38] *via* π–π stacking and hydrogen bonding interactions. Construction of PDA-based stimulus-responsive drug delivery nanosystems improves the therapeutic effect of the combination of PTT and chemotherapy.

Herein, we have devised and constructed a theranostic agent derived from copper ferrite nanospheres as the core and PDA as the shell (PDA@CFNs) for MRI guided combinatorial PTT/chemotherapy (Fig. 1). The CFNs exhibit inherently magnetic properties and high absorbance in the NIR region. As a result, they have been considered as good MRI imaging contrasts and PTT agents. The PDA shell not only improved the photothermal performances of CFNs, but also acted as the carrier of chemotherapy drugs (*e.g.*, doxorubicin, DOX, a commonly used

[a]*Department of Gastrointestinal Surgery, The First Hospital of Jilin University, 71 Xinmin Street, Changchun, Jilin 130021, People's Republic of China. E-mail: weili8308@126.com; suojian42@hotmail.com*

[b]*Department of Thyroid Surgery, The First Hospital of Jilin University, 71 Xinmin Street, Changchun, Jilin 130021, People's Republic of China*

† Electronic supplementary information (ESI) available. See DOI: 10.1039/d0ra09538a

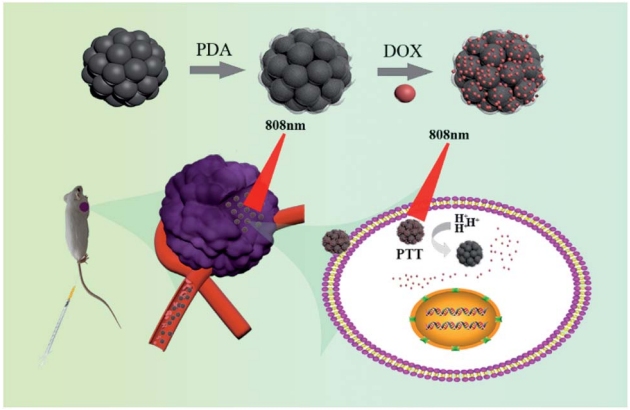

Fig. 1 Schematic illustration for the design and synthesis of PDA@CFNs-DOX for MRI-guided combined PTT and chemotherapy.

chemotherapy in clinic). Most importantly, the on-demand drug release is realized by the acidity of tumor microenvironments and NIR light irradiation. The improved therapy effect of the combination of PTT and chemotherapy and fewer side effects they induced have been proven through *in vitro* and *in vivo* evidence. Therefore, the results showed that PDA@CFNs are promising pH/NIR responsive multifunctional theranostic agents for cancer therapy.

Results and discussion

CFNs were synthesized according to the literature published earlier with minor modifications.[39] The X-ray diffraction (XRD) pattern of CFNs shows that all diffraction peaks could be well indexed to the cubic spinel structure of $CuFe_2O_4$ (JCPDS 25-0283, Fig. S1 in ESI†). As shown in the scanning electron microscopy (SEM) image and transmission electron microscope (TEM) image (Fig. 2A and B), the uniform CFNs are obtained, and the average diameter is about 100 nm. The result of X-ray

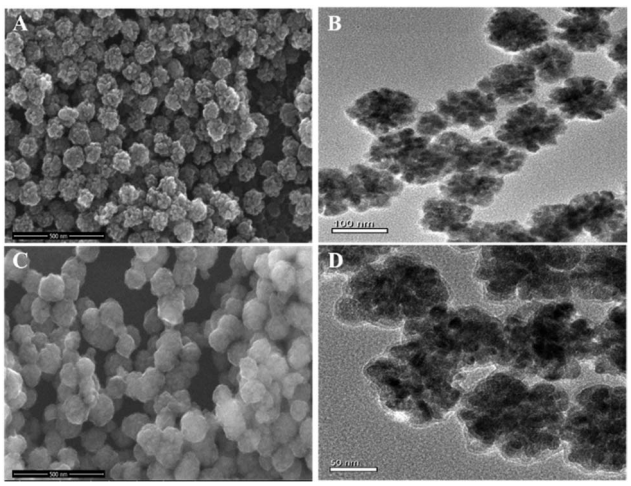

Fig. 2 (A) SEM of CFNs. (B) TEM of CFNs. (C) SEM of PDA@CFNs. (D) TEM of PDA@CFNs.

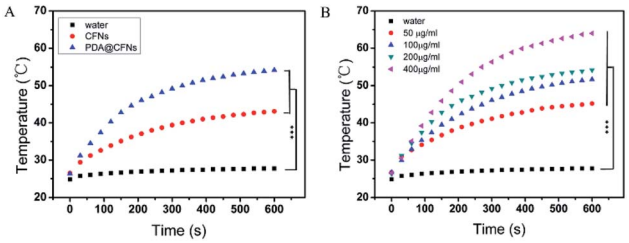

Fig. 3 (A) Plots of temperature over a period of 600 s *versus* the concentration (200 μg mL^{-1}) of CFNs and PDA@CFNs. (B) Temperature curve of different concentrations of PDA@CFNs (0, 50, 100, 200, and 400 μg mL^{-1}) under an 808 nm laser (1.5 W cm^{-2}). ***$p < 0.05$ by Student's two-tailed *t* test.

photoelectron spectroscopy (XPS) is further verified the composition of CFNs, which contains Cu, Fe, and O elements (Fig. S2†). After coating CFNs with PDA shell, the SEM and TEM images exhibit that the PDA@CFNs we obtained are still show uniform and monodispersed morphology with the thickness of the PDA shell of 25 nm (Fig. 2C and D). The appearance of the N peak in the XPS spectrum of PDA@CFNs proved that the PDA shell has been successfully coated on the surface of CFNs. Moreover, the PDA shell makes PDA@CFNs disperse well in water, and the hydrodynamic size is about 200 nm (Fig. S3†).

PDA@CFNs exhibit stronger absorbance in the near-infrared (NIR) region than that of CFNs due to the self-polymerization process of dopamine (Fig. S4†). Then we investigated the photothermal performances of CFNs and PDA@CFNs by irradiating with 808 nm laser (1.5 W cm^{-2}). Although the temperature of both CFNs and PDA@CFNs solutions increased with the irradiation time extending, PDA@CFNs displayed better photothermal conversion properties, as shown in Fig. 3A. After 600 s exposure to laser, the temperature of PDA@CFNs rapidly increased to 65 °C at the concentration of 400 μg mL^{-1}, which could kill the cancer cells effectively (Fig. 3B). Infrared thermal images further illustrate the excellent photothermal performances of PDA@CFNs (Fig. S5†). The photothermal conversion efficiency is calculated to be 38.2%, which could be attributed to the PDA shell (Fig. S6†). Such high photothermal conversion efficiency and good photothermal stability indicate PDA@CFNs are potential candidates for PTT.

Subsequently, through strong π–π stacking and hydrogen bond interaction, we loaded anti-cancer drug DOX on the surface of PDA@CFNs at a content of 648.58 μg mg^{-1}. Different pH conditions were used to study the durative release behavior of the drug. The drug release is obviously depending on the pH value as it shows in Fig. 4A. However, the release rate of DOX is still slowly even at the condition of pH 5.0, which helps in long-term continuous treatment of cancer without frequent administration. All of them achieved a faster release rate after irradiation with 808 nm laser (1.5 W cm^{-2}, 10 minutes per pulse) (Fig. 4B), indicating that the drug release of PDA@CFNs is responsive to pH and NIR laser. These results show that PDA@CFNs could act as promising smart stimuli-responsive drug delivery nanosystems for on demand chemotherapy.

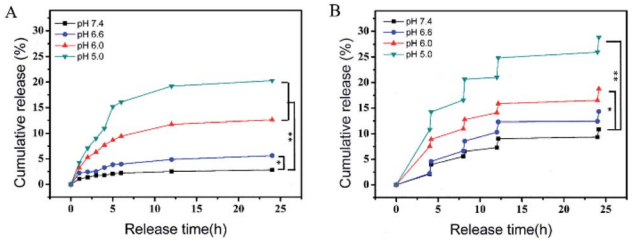

Fig. 4 (A) DOX release from PDA@CFNs-DOX at pH 7.4, pH 6.6, pH 6.0 and pH 5.0 at 37 °C. (B) NIR-triggered release of DOX from PDA@CFNs-DOX at pH 7.4, pH 6.6, pH 6.0 and pH 5.0, which were irradiated with an 808 nm NIR laser (1.5 W cm^{-2}) for 10 min at different time points. *p < 0.05 and **p < 0.01 by Student's two-tailed t test.

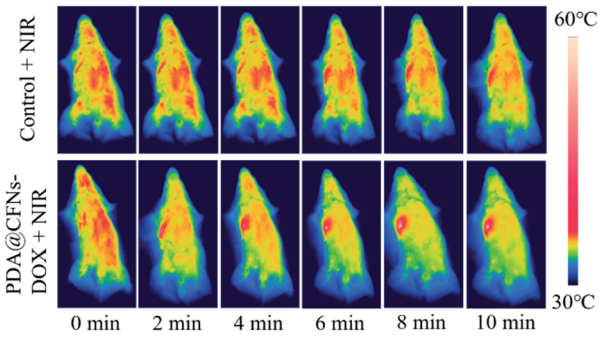

Fig. 6 *In vivo* thermal imaging of mice at 24 h after treatment with saline (control) +NIR and PDA@CFNs-DOX + NIR.

For further biological application, we evaluated the potential cytotoxicity of PDA@CFNs through CCK-8 assay using mouse colon cancer cells (CT26). As shown in Fig. 5, after CT26 cells incubating with different concentration of PDA@CFNs (from 12.5 to 200 μg mL^{-1}) for 24 h, the cell viability is close to 90% even at a high concentration of 200 μg mL^{-1}, indicating PDA@CFNs have no obvious cytotoxicity to CT26 cells. These findings illustrate that PDA@CFNs are provided with low cytotoxicity and good biocompatibility.

Inspired by the above-mentioned results, we further investigated anticancer ability of PDA@CFNs *in vitro* and *in vivo*. CT26 cells were coped with free DOX, PDA@CFNs and PDA@CFNs-DOX with and without NIR laser irradiation. PDA@CFNs-DOX showed better anticancer ability than that of free DOX as shown in Fig. 5B, which could be ascribed to that PDA@CFNs-DOX are more liable to internalization into cancer cells. It can be proved by a confocal laser scanning microscope (CLSM) (Fig. S7†). The result shows CLSM images of CT26 cells incubated with free DOX and PDA@CFNs-DOX for 0.5 h, 1 h and 3 h at 37 °C. Obviously, the stronger red fluorescence can be seen from the cells incubated with PDA@CFNs-DOX than that from free DOX, demonstrating that PDA@CFNs are good carrier for DOX. Compared with single chemotherapy and PTT, PDA@CFNs-DOX showed the most effective anticancer effect after exposed to NIR laser for 10 minutes. This result can be further proved by the live–dead cell staining technique (Fig. S8†). The significantly improved treatment effect is attributed to the excellent photothermal performances of PDA@CFNs, which can trigger and accelerate the DOX release into cells as well as kill cancer cells by photothermal effect. Importantly, the enhanced anti-cancer efficacy of chemotherapy combined with PTT can reduce side effects of chemotherapy drug.

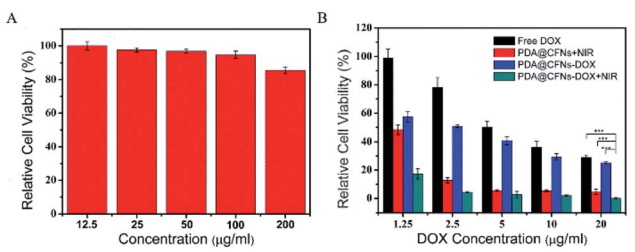

Fig. 5 (A) Cell viability of CT26 cells treated with different concentrations of PDA@CFNs (12.5, 25, 50, 100 and 200 μg mL^{-1}) determined by the CCK-8 assay. (B) Cell viability of CT26 cells incubated with free DOX, PDA@CFNs-DOX, PDA@CFNs + NIR, and CFNs @PDA-DOX + NIR. ***p < 0.001 by Student's two-tailed t test.

Subsequently, CT26 cancer cells were planted into the right axilla of female Balb/c mice to establish CT26 tumor-bearing mice model to further study the efficacy of tumor suppression. All animal procedures were performed in accordance with the Guidelines for Care and Use of Laboratory Animals of Jilin University and experiments were approved by the Animal Ethics Committee of the First Hospital of Jilin University. Then we randomly divided CT26 tumor-bearing mice into six groups: (a) saline (control group), (b) 808 nm laser (NIR group), (c) PDA@CFNs, (d) PDA@CFNs + 808 nm laser, (e) PDA@CFNs-DOX, (f) PDA@CFNs-DOX + 808 nm laser. The surface temperature changes of the tumor area irradiated with NIR laser for 10 minutes were monitored by using an infrared thermal imaging camera after the injection of PDA@CFNs-DOX. As shown in Fig. 6, the tumor temperature quickly rises above 50 °C, which is sufficient to ablate the tumor in the body. On the contrary, even when exposed to the NIR laser under the same circumstances, the tumor injected with saline did not heat up significantly. Such results indicate that PDA@CFNs-DOX has good photothermal properties *in vivo*. The tumor size and body weight of the mice were measured every other day (Fig. 7A and B). During treatment, no reduction in body weight in all groups over time, which indicates that the treatment drugs have no obvious acute toxicity. As shown in Fig. 7B, compared with the control group and laser group, the tumor growth after single chemotherapy and PTT was slightly slower, but the tumor could not be completely eliminated at the 6^{th} days. By comparison, the tumors treated with PDA@CFNs-DOX and NIR irradiation were completely eradicated within 6 days and didn't recur within 14 days (Fig. 7B and C), indicating that synergistic effect of chemotherapy and PTT have improved the therapy effect. Interestingly, the tumor of single PTT group gradually reduced and disappeared after 14 days treatment, indicating the good treatment effect of PTT, which could be ascribed to the good photothermal effect of both PDA and CFNs. The survival rates of mice of PTT/chemotherapy group and PTT group are obvious

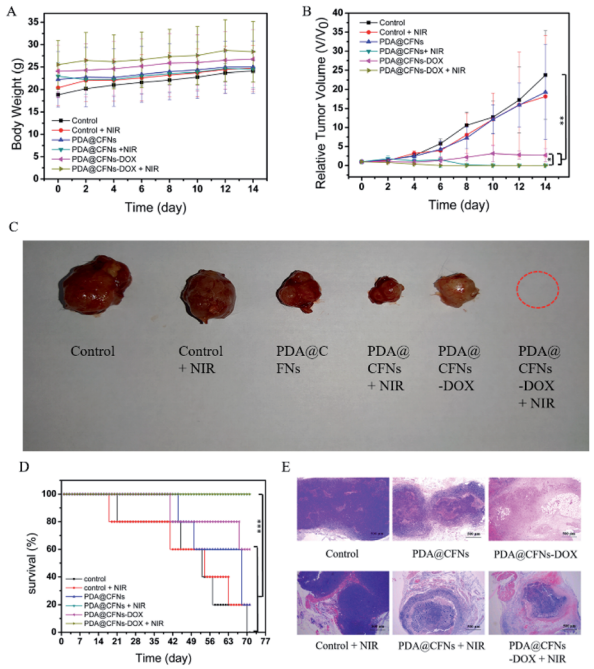

Fig. 7 (A) Body weight. (B) Relative tumor volume of the mice after treatment with saline as a control, control + NIR, PDA@CFNs, PDA@CFNs + NIR, PDA@CFNs-DOX, PDA@CFNs-DOX + NIR. (C) Photographs of excised tumors from epresentative euthanized mice after various treatments on the 6th day (D) survival rates of six groups of mice ($n = 5$) as a function of time post-treatments. (E) H&E staining of tumor slides from CT26 tumor bearing mice on the 5th day. *$p <$ 0.05, **$p < 0.01$ and ***$p < 0.001$ by wilcoxon rank sum test.

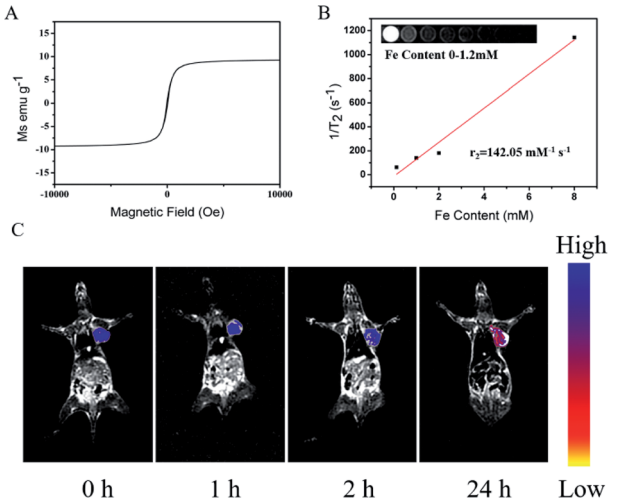

Fig. 8 (A) Magnetic hysteresis loop of the PDA@CFNs. (B) *In vitro* T_2-MRI and relaxivity plots of r_2 *versus* the different concentrations of Fe. (C) *In vivo* MRI of CT26 tumor-bearing mice before and after intravenous injection of PDA@CFNs at 0, 1, 2 and 24 h.

higher than that of other groups (Fig. 7D). In addition, the histological analysis (H&E staining) of tumor tissue further showed that compared with other treatments, synergistic PTT/chemotherapy damaged the tumor tissue more severely (Fig. 7E).

Due to their inherent paramagnetic properties (Fig. 8A), we assessed the potential of PDA@CFNs as T_2-weighted MRI contrast agent. As shown in Fig. 8B, the T_2 MRI signal intensity of PDA@CFNs decreased sharply as the Fe concentration increase, and through calculation, the value of transverse relaxation (r_2) is determined to be 142.05 mM^{-1} s^{-1}. In order to further evaluate its ability to be used as a promising contrast agent *in vivo* MR imaging, the CT26 tumor-bearing mice received a tail vein injection of PDA@CFNs. A significant blackening effect was noticed in the tumor area with the extending of injection time, as shown in Fig. 8C, indicating that PDA@CFNs can accumulate at the tumor area by enhanced permeability and retention effect (EPR).[40–42] These results prove that PDA@CFNs can be used as a T_2-weight MRI contrast agent *in vitro* and *in vivo*.

To further assess the potential of PDA@CFNs in bio-applications, we investigated their long-term toxicity after injection 30 days. The blood routine and blood biochemical analysis showed that there was no significant difference between the experiment group and control group (Fig. S9†). In addition, the main organs of the heart, liver, spleen, lung and kidney were collected and analyzed by H&E staining. As shown in Fig. S10,† no obvious tissue damage or inflammatory lesions were observed in all major organs. These results indicate that PDA@CFNs exhibit good biocompatibility and low long-term toxicity, which makes it promising as a nanothernostic agent for clinical application.

Conclusions

In summary, we successfully constructed the PDA functionalized CFNs nanocomposites for MRI-guided PTT/chemotherapy synergistic therapy. Because both CFNs and PDA have strong NIR absorption capacity, PDA@CFNs exhibit excellent photothermal performance. In addition, PDA shells enable nanocomposites act as carrier of chemotherapy drugs, and achieve pH/NIR light responsive on-demand drug release, reducing the adverse side effects of chemotherapy drugs. Compared with single PTT and chemotherapy, PDA@CFNs showed significantly improved therapeutic effects *in vitro* and *in vivo*. The high relaxivity of PDA@CFNs makes it serve as good MRI contrast agent, which provides necessary and exhaustive information for tumor diagnosis. Such good biocompatibility, high synergistic antitumor effect, and low side effects indicate PDA@CFNs promising candidates for future tumor treatments.

Author contributions

W. L. and J. S. conceived the idea and designed the experimental work. Y. D. performed research. Y. D., D. W. and W. L. analyzed the experimental data for the manuscript. Y. D. and S. W. wrote the manuscript. Y. D. and W. L. revised the manuscript.

Conflicts of interest

There are no conflicts to declare.

Acknowledgements

This work was supported by the financial aid from the National Natural Science Foundation of China (Grant No. 52072142).

Notes and references

1 L. A. Torre, R. L. Siegel, E. M. Ward and A. Jemal, *Cancer Epidemiol. Biomark. Prev.*, 2016, **25**, 16–27.
2 R. L. Siegel, K. D. Miller and A. Jemal, *Ca-Cancer J. Clin.*, 2019, **69**, 7–34.
3 V. Krishnan and A. K. Rajasekaran, *Clin. Pharmacol. Ther.*, 2014, **95**, 168–178.
4 S. W. Morton, M. J. Lee, Z. J. Deng, E. C. Dreaden, E. Siouve, K. E. Shopsowitz, N. J. Shah, M. B. Yaffe and P. T. Hammond, *Sci. Signaling*, 2014, **7**, ra44.
5 H. S. El-Sawy, A. M. Al-Abd, T. A. Ahmed, K. M. El-Say and V. P. Torchilin, *ACS Nano*, 2018, **12**, 10636–10664.
6 S. K. Joseph, M. Sabitha and S. C. Nair, *Adv. Pharm. Bull.*, 2020, **10**, 1–12.
7 M. Liu, H. Du, W. Zhang and G. Zhai, *Mater. Sci. Eng., C*, 2017, **71**, 1267–1280.
8 Y. Qiao, J. Wan, L. Zhou, W. Ma, Y. Yang, W. Luo, Z. Yu and H. Wang, Wiley interdisciplinary reviews, *Nanomed. Nanobiotechnol.*, 2019, **11**, e1527.
9 B. B. Shen, X. C. Gao, S. Y. Yu, Y. Ma and C. H. Ji, *CrystEngComm*, 2016, **18**, 1133–1138.
10 J. Liu, Y. Huang, A. Kumar, A. Tan, S. Jin, A. Mozhi and X. J. Liang, *Biotechnol. Adv.*, 2014, **32**, 693–710.
11 G. Chen, B. Yu, C. Lu, H. Zhang, Y. Shen and H. Cong, *CrystEngComm*, 2018, **20**, 7486–7491.
12 Q. Zhou, S. Shao, J. Wang, C. Xu, J. Xiang, Y. Piao, Z. Zhou, Q. Yu, J. Tang, X. Liu, Z. Gan, R. Mo, Z. Gu and Y. Shen, *Nat. Nanotechnol.*, 2019, **14**, 799–809.
13 X. Jia, J. He, L. Shen, J. Chen, Z. Wei, X. Qin, D. Niu, Y. Li and J. Shi, *Nano Lett.*, 2019, **19**, 8690–8700.
14 N. Zhang, M. Li, X. Sun, H. Jia and W. Liu, *Biomaterials*, 2018, **159**, 25–36.
15 N. S. Thakur, G. Patel, V. Kushwah, S. Jain and U. C. Banerjee, *J. Photochem. Photobiol., B*, 2019, **193**, 39–50.
16 N. S. Thakur, G. Patel, V. Kushwah, S. Jain and U. C. Banerjee, *ACS Appl. Bio Mater.*, 2019, **2**(1), 349–361.
17 Q. Dong, H. Zhang, Y. Han, A. Djamila, H. Cheng, Z. Tang, J. Zhou and Y. Ding, *J. Controlled Release*, 2018, **283**, 59–75.
18 Y. Niu, J. Zhu, Y. Li, H. Shi, Y. Gong, R. Li, Q. Huo, T. Ma and Y. Liu, *J. Controlled Release*, 2018, **277**, 35–47.
19 R. Li and Y. Xie, *J. Controlled Release*, 2017, **251**, 49–67.
20 L. Wang, M. Huo, Y. Chen and J. Shi, *Adv. Healthcare Mater.*, 2018, **7**, e1701156.
21 B. S. Gong, R. Wang, H. X. Xu, M. Y. Miao and Z. Z. Yao, *Curr. Cancer Drug Targets*, 2019, **19**, 525–533.
22 X. Lei, Y. Lei, J. K. Li, W. X. Du, R. G. Li, J. Yang, J. Li, F. Li and H. B. Tan, *Cancer Lett.*, 2020, **470**, 126–133.
23 A. C. V. Doughty, A. R. Hoover, E. Layton, C. K. Murray, E. W. Howard and W. R. Chen, *Materials*, 2019, **12**, 779.
24 Y. Liu, P. Bhattarai, Z. Dai and X. Chen, *Chem. Soc. Rev.*, 2019, **48**, 2053–2108.
25 E. A. Hussein, M. M. Zagho, G. K. Nasrallah and A. A. Elzatahry, *Int. J. Nanomed.*, 2018, **13**, 2897–2906.
26 K. Sztandera and M. Gorzkiewicz, *Mol. Pharmaceutics*, 2019, **16**, 1–23.
27 B. Navyatha and S. Nara, *Nanomedicine*, 2019, **14**, 766–796.
28 Y. Liu, M. Ji and P. Wang, *Mol. Pharmaceutics*, 2019, **16**, 3322–3332.
29 X. Huang, C. Xu, Y. Li, H. Cheng, X. Wang and R. Sun, *Mater. Sci. Eng., C*, 2019, **96**, 129–137.
30 C. Zhang, W. Bu, D. Ni, C. Zuo, C. Cheng, Q. Li, L. Zhang, Z. Wang and J. Shi, *J. Am. Chem. Soc.*, 2016, **138**, 8156–8164.
31 A. Sharma and J. Das, *J. Nanobiotechnol.*, 2019, **17**, 92.
32 K. Yang, L. Feng, X. Shi and Z. Liu, *Chem. Soc. Rev.*, 2013, **42**, 530–547.
33 Z. Guo, M. Chen, C. Peng, S. Mo, C. Shi, G. Fu, X. Wen, R. Zhuang, X. Su, T. Liu, N. Zheng and X. Zhang, *Biomaterials*, 2018, **179**, 134–143.
34 Y. W. Jiang, G. Gao, P. Hu, J. B. Liu, Y. Guo, X. Zhang, X. W. Yu, F. G. Wu and X. Lu, *Nanoscale*, 2020, **12**, 210–219.
35 Y. Liu, K. Ai, J. Liu, M. Deng, Y. He and L. Lu, *Adv. Mater.*, 2013, **25**, 1353–1359.
36 J. Stritzker, L. Kirscher, M. Scadeng, N. C. Deliolanis, S. Morscher, P. Symvoulidis, K. Schaefer, Q. Zhang, L. Buckel, M. Hess, U. Donat, W. G. Bradley, V. Ntziachristos and A. A. Szalay, *Proc. Natl. Acad. Sci. U. S. A.*, 2013, **110**, 3316–3320.
37 R. S. Ambekar and B. Kandasubramanian, *Biomater. Sci.*, 2019, **7**, 1776–1793.
38 R. Mrówczyński, *ACS Appl. Mater. Interfaces*, 2018, **10**, 7541–7561.
39 Y. Liu, W. Zhen, L. Jin, S. Zhang and G. Sun, *ACS Nano*, 2018, **12**, 4886–4893.
40 D. W. Bartlett, H. Su, I. J. Hildebrandt, W. A. Weber and M. E. Davis, *Proc. Natl. Acad. Sci. U. S. A.*, 2007, **104**, 15549–15554.
41 F. Chen, H. Hong, S. Goel, S. A. Graves, H. Orbay, E. B. Ehlerding, S. Shi, C. P. Theuer, R. J. Nickles and W. Cai, *ACS Nano*, 2015, **9**, 3926–3934.
42 G. Ku, M. Zhou, S. Song, Q. Huang, J. Hazle and C. Li, *ACS Nano*, 2012, **6**, 7489–7496.